Nano-Mole Scale Side-Chain Signal Assignment by [1]H-Detected Protein Solid-State NMR by Ultra-Fast Magic-Angle Spinning and Stereo-Array Isotope Labeling

Songlin Wang[1ʘ], Sudhakar Parthasarathy[1ʘ], Yusuke Nishiyama[2,3], Yuki Endo[2], Takahiro Nemoto[2], Kazuo Yamauchi[4,5], Tetsuo Asakura[6], Mitsuhiro Takeda[7], Tsutomu Terauchi[8], Masatsune Kainosho[7,9], Yoshitaka Ishii[1,10]*

1 Department of Chemistry and University of Illinois at Chicago, Chicago, Illinois, United States of America, 2 JEOL RESONANCE Inc., Akishima, Tokyo, Japan, 3 RIKEN CLST-JEOL collaboration center, RIKEN, Yokohama, Kanagawa, Japan, 4 School of Science and Technology, Nazarbayev University, Astana, Kazakhstan, 5 Nuclear Magnetic Resonance Core Lab., King Abdullah University of Science and Technology, Thuwal, Saudi Arabia, 6 Department of Biotechnology, Tokyo University of Agriculture and Technology, Koganei, Tokyo, Japan, 7 Structural Biology Research Center, Graduate School of Science, Furocho, Chikusa-ku, Nagoya University, Nagoya, Japan 464–8601, 8 SAIL Technologies Co., Inc., Tsurumi-ku, Yokohama, Kanagawa, Japan, 9 Center for Priority Areas, Tokyo Metropolitan University, Tokyo, Japan, 10 Center for Structural Biology, University of Illinois at Chicago, Chicago, Illinois, United States of America

ʘ These authors contributed equally to this work.
* yishii@uic.edu

Abstract

We present a general approach in [1]H-detected ^{13}C solid-state NMR (SSNMR) for side-chain signal assignments of 10-50 nmol quantities of proteins using a combination of a high magnetic field, ultra-fast magic-angle spinning (MAS) at ~80 kHz, and stereo-array-isotope-labeled (SAIL) proteins [Kainosho M. et al., Nature **440**, 52–57, 2006]. First, we demonstrate that ^{1}H indirect detection improves the sensitivity and resolution of ^{13}C SSNMR of SAIL proteins for side-chain assignments in the ultra-fast MAS condition. ^{1}H-detected SSNMR was performed for micro-crystalline ubiquitin (~55 nmol or ~0.5mg) that was SAIL-labeled at seven isoleucine (Ile) residues. Sensitivity was dramatically improved by ^{1}H-detected 2D ^{1}H/^{13}C SSNMR by factors of 5.4-9.7 and 2.1-5.0, respectively, over ^{13}C-detected 2D ^{1}H/^{13}C SSNMR and 1D ^{13}C CPMAS, demonstrating that 2D ^{1}H-detected SSNMR offers not only additional resolution but also sensitivity advantage over 1D ^{13}C detection for the first time. High ^{1}H resolution for the SAIL-labeled side-chain residues offered reasonable resolution even in the 2D data. A [1]H-detected 3D ^{13}C/^{13}C/^{1}H experiment on SAIL-ubiquitin provided nearly complete ^{1}H and ^{13}C assignments for seven Ile residues only within ~2.5 h. The results demonstrate the feasibility of side-chain signal assignment in this approach for as little as 10 nmol of a protein sample within ~3 days. The approach is likely applicable to a variety of proteins of biological interest without any requirements of highly efficient protein expression systems.

Introduction

[1]H indirect detection was introduced to ^{13}C and ^{15}N biomolecular high-resolution solid-state NMR (SSNMR) about a decade ago. [1–4] Despite its potential as a powerful tool to enhance sensitivity and resolution, ^{1}H-detected SSNMR is not widely used due to limits on ^{1}H resolution, even under fast MAS, and the lack of a demonstrated sensitivity advantage over more commonly used ^{13}C detection. The recent introduction of ^{1}H dilution by high-level deuteration and partial back-exchange of amide [1]H (10–20%) has greatly improved the resolution of ^{1}H SSNMR for biomolecules,[5, 6] offering a practical protocol for ^{1}H indirect detection in protein SSNMR. However, the method is limited by a gross loss of ^{1}H signals from amide sites (80–90%) due to extensive deuteration. ^{1}H-detected ^{13}C SSNMR for a fully protonated protein at very fast MAS (~40 kHz) has been used to obtain signal assignments for a model protein. [7] Nevertheless, this method is still hampered by relatively broad ^{1}H line widths (0.5–1 ppm), a resolution that is insufficient even for small proteins. More importantly, it has been difficult to improve the sensitivity of 2D ^{1}H indirect detection over that of standard 1D ^{13}C direct-detected SSNMR. Recent studies described ^{1}H indirect detection under ultra-fast MAS (UFMAS) at spinning frequencies of 60 kHz, resulting in resolved amide ^{1}H resonances for fully deuterated proteins with fully back-exchanged amide proton[8, 9] or for undeuterated proteins. [10] Although those studies demonstrated the feasibility of main-chain sequential assignments for micro-crystalline samples, no strategy for assigning side-chain resonances by ^{1}H-detected SSNMR has yet been developed, despite the fundamental importance of side chain structures and dynamics for protein functions. Equally importantly, no previous studies established advantage of ^{1}H indirect detection method over traditional ^{13}C direct detection for concurrent improvement in sensitivity and resolution by a quantitative analysis. Although some previous studies demonstrated sensitivity advantage of 2D ^{1}H-detected SSNMR over 2D ^{13}C-detected SSNMR,[7, 11, 12] it was difficult to achieve sensitivity advantage by [1]H-detected (*N*+1)-dimensional SSNMR over a corresponding *N*-dimensional ^{13}C-detected SSNMR scheme with an additional ^{1}H dimension for higher resolution (*N* = 1, 2..). To overcome these problems, in this study, we propose the use of stereo-array isotope labeling (SAIL) as a highly effective labeling scheme suitable for side-chain signal assignments by ^{1}H-detected protein SSNMR. The SAIL scheme was originally introduced to overcome the size limitation of biomolecular solution NMR by incorporating stereo-selective deuteration to achieve isolated ^{1}H throughout all side chains of a protein.[13] Although ^{1}H SSNMR was attempted for a SAIL amino acid (L-valine) under fast MAS at ~30 kHz,[14] resultant ^{1}H line widths were still in a range of 0.5–0.7 ppm; the limited ^{1}H resolution has hampered successful use of SAIL labeling for protein SSNMR. In addition, it is not trivial to determine whether sufficient sensitivity can be achieved for a SAIL-labeled protein sample under UFMAS conditions for limited sample quantity in a smaller MAS rotor and potentially much longer [1]H T_1 values due to deuteration. In this work, we demonstrate that a combination of UFMAS and SAIL selective deuteration significantly improves the sensitivity of ^{1}H-detected 2D ^{13}C SSNMR of biomolecules over 1D and 2D ^{13}C direct detection. It is also discussed that this combination offers extremely sensitive means of biomolecular SSNMR for side-chain assignments with resolution enhanced ^{1}H signals having line widths of 0.1–0.2 ppm.

Results and Discussion

First, in experiments on amino-acid samples, we investigated whether the combined use of SAIL labeling with UFMAS in a high magnetic field of 17.62 T (^{1}H frequency of 750.15 MHz) could improve the resolution of ^{1}H SSNMR resolution. Fig 1(a, b) shows chemical structures and labeling schemes for (a) uniformly [13]C- and ^{15}N-labeled isoleucine (UL-Ile) and (b)
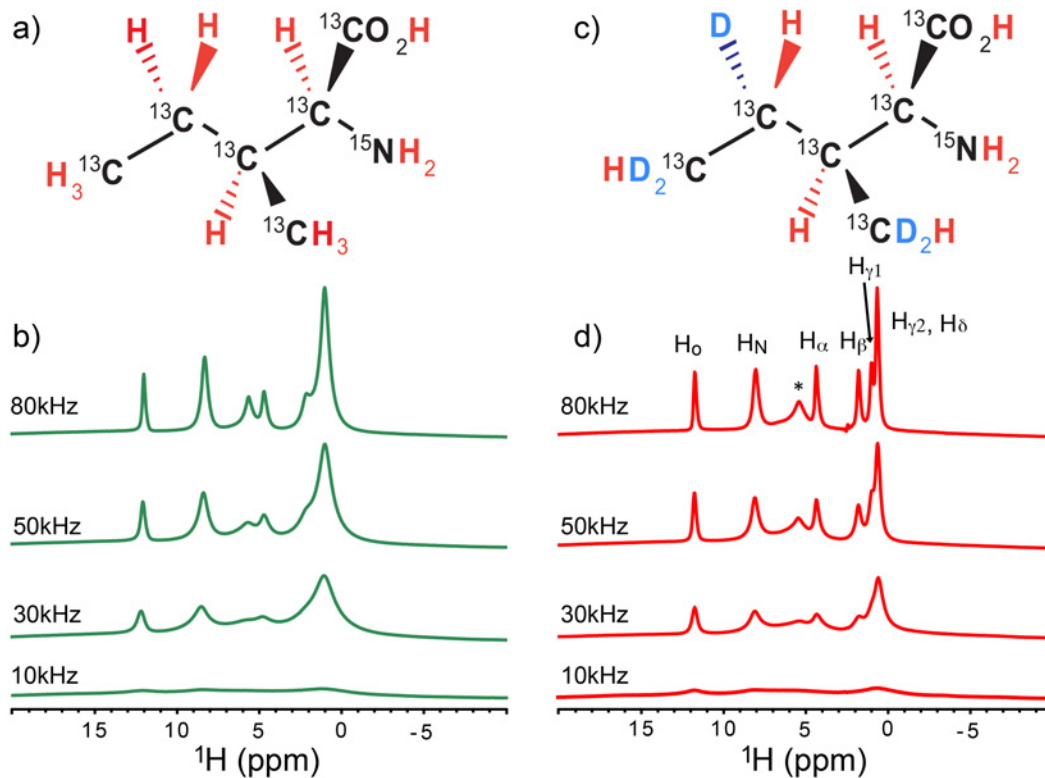
Fig 1. Spinning-speed dependence of 1H MAS spectra of fully protonated and SAIL isoleucine samples. (a, b) Chemical structures of (a) uniformly [13]C- and ^{15}N-labeled (UL) Ile and (b) SAIL-Ile. (c, d) Spinning-speed dependence of ^{1}H MAS SSNMR spectra of (c) UL-Ile and (d) SAIL-Ile. The peak at 4.8 ppm (*) is likely due to HCl salts.[17, 18] No window functions were applied.

SAIL-isoleucine (SAIL-Ile). Unlike random deuteration, in a SAIL scheme, all the protonated ^{13}C groups are connected to a single ^{1}H species. This feature allows preparation of strong ^{13}C polarization for all ^{13}C species via efficient double-quantum cross-polarization from directly bonded ^{1}H nuclei.[15] More importantly, isolated ^{1}H spins allow us to achieve very high resolution without the effects of strong [1]H–[1]H dipolar couplings. Fig 1(c, d) shows the spinning-speed dependence of ^{1}H MAS SSNMR of (c) UL-Ile and (d) SAIL-Ile, with signal assignments provided in (d). Significant improvement in resolution and sensitivity was obtained at higher spinning speeds (ν_R). Resolution enhancements of 2–3-fold were observed at $\nu_R = 80$ kHz in (d) relative to $\nu_R = 30$ kHz, which was used in previous studies of ^{1}H SSNMR on SAIL-valine. [14] Clearly, SAIL-Ile provided much higher resolution in Fig 1d ($\nu_R = 80$ kHz) relative to the corresponding spectrum for UL-Ile in Fig 1c. In particular, for H_β, H_γ, and H_δ groups, the spectrum for SAIL-Ile exhibits a dramatic improvement in resolution (by a factor of 3–4) relative to the resolution for UL-Ile, with ^{1}H widths of 0.21–0.25 ppm at 80 kHz. This narrowing can be attributed to the isolation of ^{1}H in methylene and methyl groups by stereo-specific deuteration in the SAIL scheme.[13, 16] Much broader ^{1}H line widths (0.7–1.0 ppm) were observed for these groups in UL-Ile (Fig 1c). These observations confirm that UFMAS itself is still not sufficient to remove broadening due to strong [1]H–[1]H dipolar couplings within the CH_2 and CH_3 groups, even at ν_R of ~80 kHz. The combination of SAIL and UFMAS also exhibited modest narrowing (15–20%) in the line widths of O–H (0.22 ppm) and [1]H_α (0.26 ppm) (Fig 1d). We also confirmed the excellent ^{1}H resolution at ν_R of ~80 kHz for SAIL Thr (Fig A in S1 File).

The sensitivity enhancement factor (ξ) of ^{1}H indirect detection over direct detection of a dilute X nuclei depends on the line width in the ^{1}H dimension W_H, the apodization, and the efficiency of polarization transfer (f) from X to ^{1}H used for ^{1}H detection, as shown in Eq (1),[1, 2]

$$\xi = \frac{f}{\sqrt{\alpha}} \left(\frac{\gamma_H}{\gamma_X}\right)^{3/2} \left(\frac{W_X}{W_H}\right)^{1/2} \left(\frac{Q_X}{Q_H}\right)^{1/2},$$

(1)

where γ_H and γ_X represent the gyromagnetic ratios of the nuclei H and X, W_H and W_X are the line widths observed for ^{1}H and X nuclei, and Q_H and Q_X are the quality factors for the sample coil for ^{1}H and X detection, respectively. The factor α is 1 for a comparison of 2D ^{1}H-detected X/^{1}H correlation SSNMR with 2D X-detected X/^{1}H correlation. For a comparison of 2D ^{1}H-detected X/^{1}H correlation with 1D ^{13}C CPMAS, the α value becomes 2π assuming apodization with matched window functions (see SI about the details).[1, 2] Thus, there is a ~2.5-fold difference (i.e., $\sqrt{2\pi}$) between the ξ values of the 1D and 2D direct X-detection experiments. In biomolecular SSNMR, it is typical that no or minimal line broadening is applied for higher spectral resolution. When no window functions are applied in the ^{1}H dimension, $\alpha \sim 2\pi^2$ for the comparison with 1D ^{13}C SSNMR; thus, this suggests a 4.4-fold difference (i.e., $\sqrt{2}\pi$) between the ξ values for 1D and 2D (see SI about the details). Compared with the ^{1}H resolution for UL-Ile at $\nu_R = 40$ kHz, which was previously used in ^{1}H-detected protein SSNMR, [7] the ^{1}H resolution for CHD and CHD$_2$ groups improved as much as 5–6-fold for the SAIL sample at $\nu_R = 80$ kHz. We confirmed that the transfer efficiency f by ^{1}H–^{13}C double-quantum CP at $\nu_R = 80$ kHz was comparable to the CP efficiency at $\nu_R = 20$–40 kHz for SAIL-Ile. Thus, this new combination of SAIL and UFMAS offers opportunities to dramatically improve the sensitivity and resolution of ^{1}H detection.

Next, we explored the possibility of improving the sensitivity and resolution of ^{13}C SSNMR for SAIL proteins. As a suitable benchmark, we selected a micro-crystalline sample of ubiquitin (Ubq) that was selectively labeled with SAIL-Ile to compare the resolution with that of the amino acid data. Because there are as many as seven Ile residues in ubiquitin, the system is also suited for investigating improvements in the resolution of ^{1}H detection. Another major challenge is the limited amount of sample used in these experiments. Because the engineering needs for UFMAS at 80 kHz limit the sample volume to only ~1 μL, it was difficult to achieve sufficient sensitivity in multi-dimensional ^{13}C protein SSNMR, even in a high magnetic field. Fig 2a and 2b shows (a) ^{1}H-detected and (b) ^{13}C-detected 2D ^{13}C/^{1}H correlation spectra of the SAIL-Ubq sample. In the ^{1}H-detected 2D spectrum, the sensitivity was dramatically improved (by a factor of 5.4–9.7) (Fig 2a) relative to the ^{13}C-detected 2D data (b), as shown from the comparison of the slices corresponding to the peaks indicated by arrows (d–g). The factors were confirmed with the data collected from additional scans for (b) (see Table A in S1 File). As a result of this significant improvement, the 2D spectrum in Fig 2a was obtained after only 5 min, using sub-milligram quantities of protein sample (~0.5 mg or ~55 nmol, excluding H$_2$O). By contrast, the corresponding ^{13}C-detected 2D spectrum in Fig 2b had a much lower signal-to-noise ratio. Because of the excellent ^{1}H resolution, most of the resonances are well separated in the ^{1}H-detected 2D spectrum in Fig 2a in contrast to the significant signal overlap observed in the 1D ^{13}C SSNMR in (c). It should be noted that the backbone ^{13}Cα signals and some of the ^{13}Cβ signals were weak because the protein was expressed in a D$_2$O medium and, consequently, ^{1}Hα and some ^{1}Hβ were replaced by ^{2}H; this issue can be overcome by expressing the protein in a cell-free system. It is also noteworthy that only 7.5 mg of SAIL-Ile was needed for preparing the sample at high labeling efficiency (~90%) from an E. coli cell culture of 0.5 L. The ^{1}H line widths were 0.14–0.25 ppm and 0.10–0.22 ppm, respectively, with and
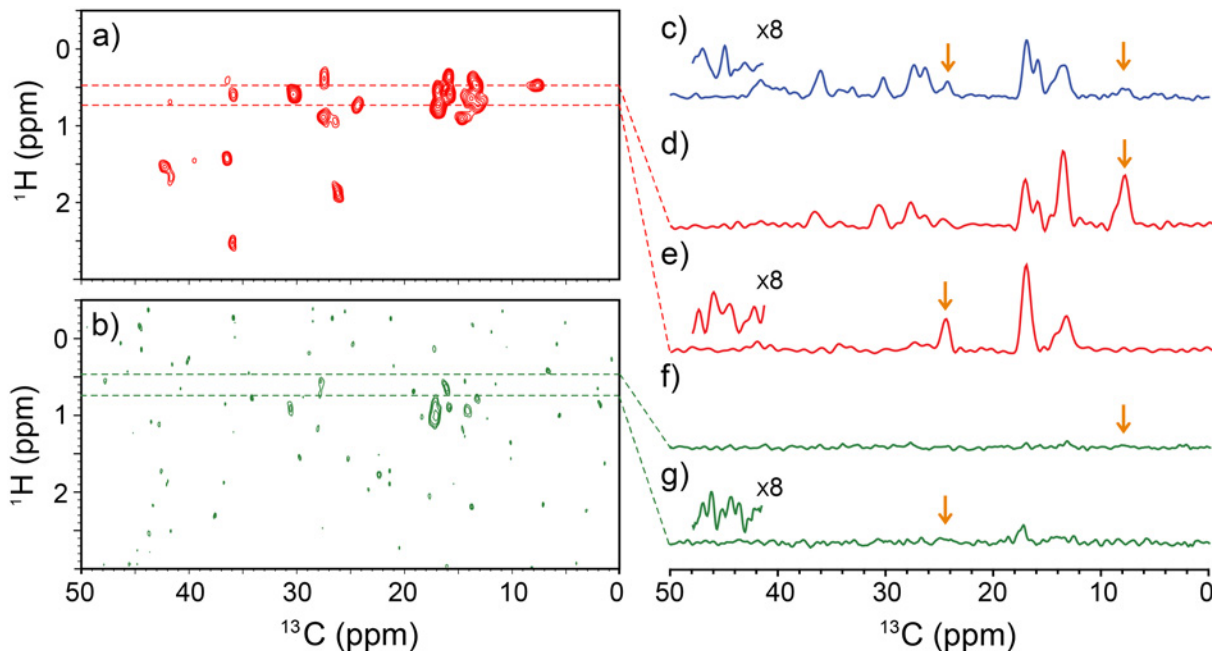
Fig 2. A comparison of 1H-detected and 13C-detected 2D and 1D SSNMR spectra of SAIL ubiquitin. (a) ^{1}H-detected and (b) ^{13}C-detected 2D ^{13}C/^{1}H spectra and (c) a 1D ^{13}C CP-MAS spectrum of SAIL-Ubq (~0.5 mg) at MAS 80 kHz. (d–g) 1D slices from ^{1}H shifts of (d, f) 0.43 ppm and (e, g) 0.69 ppm from (d, f) ^{1}H-detected and (e, g) ^{13}C-detected experiments. All spectra were processed with 45°- and 60°-shifted sine-bell window functions in the ^{1}H and ^{13}C dimensions, respectively. The ^{1}H and ^{13}C line widths were 0.10–0.22 ppm and 0.66–0.94 ppm, respectively, in the absence of any window functions. The insets in (c, e, and g) show the magnified noise regions. Each spectrum in (a–c) was collected within ~5 min. The pulse sequences used for (a) and (b) are shown in Fig B and Fig C in S1 File.

doi:10.1371/journal.pone.0122714.g002

without window functions. Clearly, our approach has opened an avenue for micro-SSNMR analysis of a protein sample in a minimal experimental time.

The sensitivity enhancement factors by ^{1}H-detected data in (d, e) relative to 1D ^{13}C CPMAS in (c) for resolved ^{13}CHD signals at 24.5 ppm and ^{13}CHD$_2$ signals at 7.9 ppm (orange arrows) were 2.1 and 5.0, respectively. These factors are slightly greater than the theoretical values 1.5–2.7, which were obtained by multiplying $\sqrt{1.5}/(\sqrt{2}\pi)$ by the experimental ξ values for the ^{13}C-detected 2D experiment, where the factor $1/\sqrt{2}\pi$ came from the sensitivity difference between 2D and 1D experiments without window functions (see SI). The modest gain by a factor of $\sqrt{1.5}$ (or ~1.2) was expected from "time saving" due to a linear prediction, (LP) which was employed to extend the indirect time-domain signals by 1.5 fold although an apparent S/N ratio with LP may be influenced by other issues such as additional "noise" for prediction artifacts. We also experimentally confirmed similar sensitivity improvement factors ξ over 1D CPMAS (ξ = 1.3–2.0) and ^{13}C-detected 2D correlation (ξ = 3.9–10.1) for SAIL-Ile (see Fig E and Table B in S1 File). To the best of our knowledge, this is the first demonstration that ^{1}H-detected 2D ^{1}H/^{13}C correlation SSNMR for a protein sample is significantly more sensitive than 1D ^{13}C direct detection.

The results described above suggest that most standard ^{13}C-detected 2D and 3D SSNMR involving side-chain signals can be replaced by ^{1}H-detected 3D and 4D SSNMR, respectively, with significantly enhanced *resolution and sensitivity*. To test this possibility, we performed ^{1}H-detected 3D ^{13}C/^{13}C/^{1}H correlation SSNMR on the SAIL-Ubq sample. Fig 3 shows (a,b) a 2D ^{13}C/^{13}C projection of the 3D data and (c–e) strip plots of ^{13}C/^{13}C 2D slices corresponding to ^{1}H chemical shifts of (c) 1.57 ppm, (d) 1.73 ppm, and (e) 1.41 ppm. The 3D spectrum in
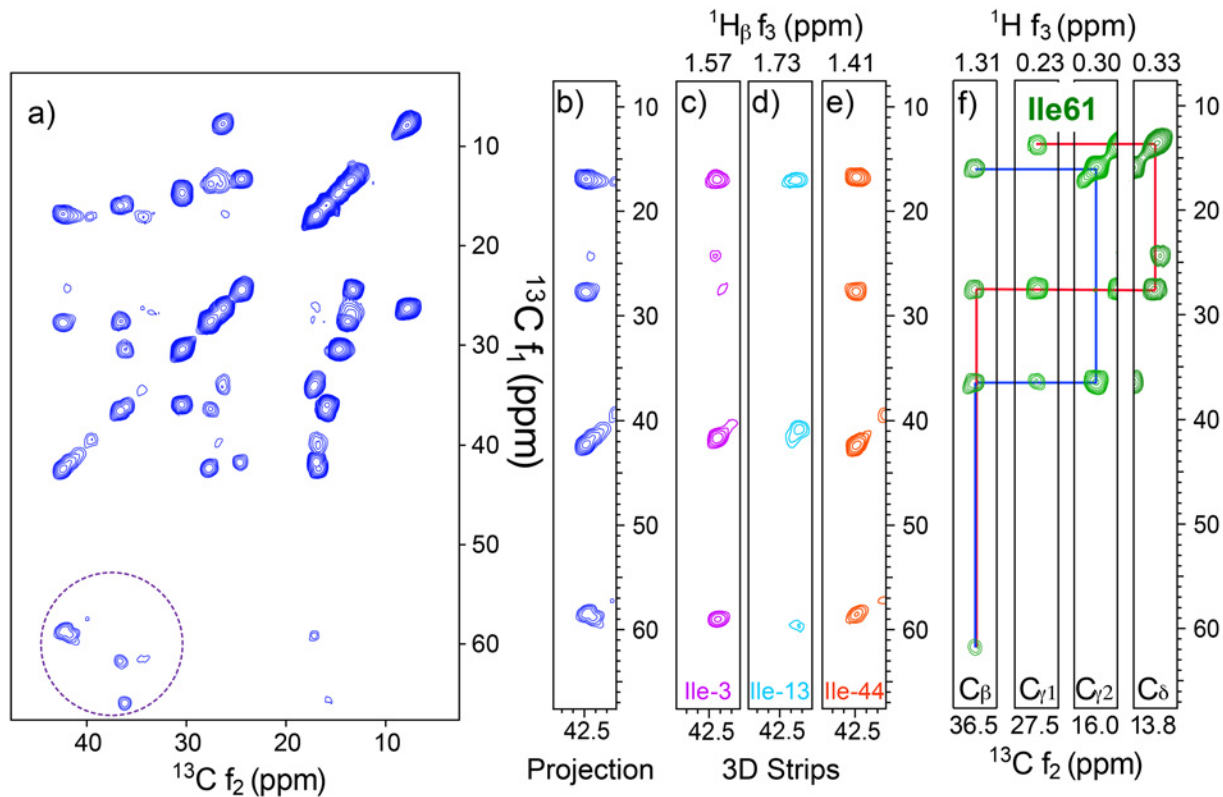
Fig 3. Resolution and side-chain assignments from 3D ^{13}C/^{13}C/^{1}H SSNMR of SAIL-Ubq. (a, b) 2D ^{13}C/^{13}C 2D projection spectra from a ^{1}H-detected 3D ^{13}C/^{13}C/^{1}H SSNMR of SAIL-Ubq at MAS 80 kHz. All the peaks including minor ones in (a) are attributed to intra-residue cross peaks within the Ile residues. (c–e) Representative 2D ^{13}C/^{13}C slices corresponding to ^{1}H chemical shifts of (c) 1.57 ppm, (d) 1.73 ppm, and (e) 1.41 ppm. The data show clear separation of signals for (c) Ile-3, (d) Ile-13, and (e) Ile-44 by ^{1}H shifts. The spectrum was processed with 45°- and 60°-shifted sine-bell window functions in the ^{1}H and ^{13}C dimensions, respectively. (f) ^{13}C/^{1}H assignments for Ile-61 from the 3D data. The pulse sequence is listed in Fig D in S1 File.

doi:10.1371/journal.pone.0122714.g003

Fig 3 was obtained in 2.5 h, despite the deuteration of C_α and partial deuteration of C_β. We did not attempt a 3D experiment by ^{13}C detection, as it would have taken up to 10 days. All the ^{13}C resonances for the seven Ile residues are observed in Fig 3a, including those for nearly fully deuterated ^{13}C$_\alpha$ (dotted circle). These ^{13}C$_\alpha$ resonances were detected in the t_1 period by polarization transfer from remote ^{1}H, correlation to ^{13}C$_\beta$ in t_2, and final detection at ^{1}H$_\beta$ in the t_3 period. In the 2D ^{13}C/^{13}C projection, the signal overlap could not be completely eliminated. For example, the three signals for Ile-3, Ile-13, and Ile-44 are nearly overlapping at $(f_1, f_2) \sim$ (59 ppm, 42 ppm) in the projection shown in Fig 3b. However, in 2D slices at three different ^{1}H shifts (Fig 3c–3e), these overlapped peaks are clearly separated by well dispersed ^{1}H$_\beta$ shifts. All the side-chain ^{1}H and ^{13}C resonances of Ile, except for ^{1}H$_{\gamma 1}$ of Ile-13, were assigned with excellent resolution (Table C in S1 File), as shown for an example of Ile-61 in Fig 3f. Although the ^{13}C$_\alpha$ and ^{13}C$_\beta$ signals were assigned here to specific residues based on previous ^{13}C-detected SSNMR studies,[19, 20] it is possible to connect side-chain resonances to main-chain and ^{13}C$_\beta$ resonances, which can be assigned from ^{1}H-detected SSNMR for a uniformly ^{13}C- and ^{15}N-labeled protein as previously discussed. [10] It should be noted that the main-chain assignment strategy by ^{1}H-detection [10] is likely to be applicable to uniformly SAIL-labeled proteins. In that case, spectral assignments for the main chain as well as side chains could be obtained by the ^{1}H-detection method on the uniformly SAIL-labeled protein. Alternatively, site-directed mutagenesis can be used for assignments of some specific residues. Thus, the

^{1}H-detected high-field SSNMR approach using SAIL-labeled protein and UFMAS is highly effective for side-chain assignments. The data suggest that side-chain assignments by 3D SSNMR analysis can be obtained from 10 nmol (or ~90 μg for Ubq) within only ~3 days in our approach.

Conclusion

In this work, we discussed a general approach to achieve side-chain spectral assignments of SAIL-labeled proteins by ^{1}H-detected protein SSNMR approaches. This work raises new prospects for high-field protein SSNMR in two areas. First, we presented the advantage of ^{1}H-detected high-field SSNMR by demonstrating feasibility of side-chain assignments from 10–50 nmol of SAIL-labeled proteins under UFMAS at 80 kHz. To date no approach has been able to achieve efficient side-chain assignments through ^{1}H-detected biomolecular SSNMR. Our data clearly demonstrate that, using this approach, heavily overlapped ^{13}C side-chain signals can be resolved by ^{1}H shifts for all seven Ile residues in SAIL-labeled ubiquitin with minimal sample requirements. Unlike methyl-selective labeling,[21] ^{1}H-detected SSNMR for SAIL-labeled proteins offers [13]C–[13]C connectivities and high-resolution ^{1}H SSNMR for stereo-selectively labeled CHD groups for side-chain assignments. The method can be applied to structural analyses of a variety of proteins that are either selectively labeled with a set of different SAIL amino acids or uniformly labeled with SAIL amino acids. Although preparation of a SAIL-labeled protein in the large quantities required for conventional SSNMR experiments (0.5–1 μmol) is cost-prohibitive, the minimal sample requirement (10–50 nmol) of our approach makes such an approach very practical. The demonstrated reduction of sample requirements will make it feasible to implement even more advanced isotope labeling schemes or multiple sets of differently SAIL-labeled samples for future biomolecular SSNMR.

Secondly, we experimentally demonstrated that ^{1}H indirect detection in 2D–3D SSNMR experiments on the SAIL-labeled protein notably improved sensitivity as well as additional ^{1}H spectral resolution, over traditional ^{13}C-direct detection in the corresponding 1D–2D experiments. This suggests that in our approach combining uses of UFMAS at 80 kHz and SAIL proteins, many of traditional 2D-3D ^{13}C-detected experiments can be replaced by [1]H-detected 3D-4D experiments. As discussed above, in most of previous studies the sensitivity advantage of ^{1}H indirect detected SSNMR was described for less useful ^{15}N SSNMR, rather than for ^{13}C SSNMR, which is 4-fold more sensitive. In this work, we quantitatively demonstrated the sensitivity and resolution advantage of this method over traditional ^{13}C-detected SSNMR in a high field (17.6 T), which is now widely available to the scientific community. We reported up to 10-fold sensitivity improvements by ^{1}H detection and UFMAS at 80 kHz when a [1]H-detected 2D–3D experiment is compared with an equivalent ^{13}C-detected 2D–3D experiment. It will be feasible to reach the detection limit of a few nmol or sub-nmol of SAIL-labeled proteins by further sensitivity enhancement using paramagnetic doping[19, 22], modified polarization transfer schemes,[23], non-uniform sampling[24], and even faster MAS.[15, 25, 26] This approach is likely to applicable to a variety of micro/nano-crystalline proteins in order to drastically speed up side-chain spectral and structural analysis. Although it is outside the scope of this study, a similar approach using [1]H- or ^{19}F-detection should be possible for amyloid aggregates with reasonable structural homogeneity[27–33] and bioinorganic samples.[34, 35]

Materials and Methods

The SAIL-Ile and UL-Ile used for these experiments were recrystallized in 20% DCl in D_2O[17] before packing into a MAS rotor. SAIL-Ubq samples were expressed in *E. coli* BL21 cells harboring a plasmid containing the chlorella Ubq gene, cultured in D_2O/M9 medium supplemented

with SAIL-Ile, as described in the SI. The sample was crystallized by dissolving 2 mg of the lyophilized powder in 160 μL of citrate buffer in D_2O and then precipitating with 240 μL d_{12}-MPD (2-methyl-2,4-pentanediol).[20] Further details about the sample preparation are discussed in the SI.

All SSNMR experiments were performed on a Bruker Avance III 750MHz spectrometer at the UIC Center for Structural Biology using a JEOL 1 mm $^1H/^{13}C/^{15}N/^2H$ quad-resonance MAS probe. All the ^{13}C–^1H polarization transfers in this work were performed using adiabatic double-quantum cross-polarization (DQ-CP) schemes[19, 36], with the sum of the rf field strengths for I and S hetero-nuclear spins matched to ω_R (i.e., $\omega_{1I} + \omega_{1S} = \omega_R$) so that sample heating was minimized at high repetition rates by the low-power CP scheme.[10, 15] For ^1H decoupling, a low-power decoupling scheme[37] with SPINAL-64[38] at 10 kHz was applied. For ^{13}C, ^{15}N, and ^2H decoupling, a WALTZ-16 scheme was used at RF field strengths of 10, 2, and 5 kHz, respectively. All the multi-dimensional NMR data were processed using the nmrPipe software.[39] Unless stated otherwise, all indirect time-domain signals in the 2D and 3D data were extended to 1.5-fold and 2-fold by linear prediction, respectively. The multi-dimensional SSNMR data were apodized with 45°- and 60°-shifted sine-bell window functions in the ^1H and ^{13}C dimensions, respectively, to balance sensitivity and resolution. For the SAIL-Ile and Ubq samples, ^{13}C decoupling was applied during the ^1H detection/evolution periods, whereas the ^1H and ^2H decoupling sequences were applied during the ^{13}C detection/evolution periods. For the SAIL samples, the sample temperature under UFMAS at 80 kHz was kept at ~37°C using a FTS cooler unit with N_2 gas at −12°C.

The ^1H NMR spectra in Fig 1 were collected with π/2-pulse direct excitation with WALTZ-16 ^{13}C decoupling [3] at an RF field strength of 10 kHz with a recycle delay of 10 s. The details of the pulse sequences used for Figs 2 and 3 are listed in the SI (Figs B–D in S1 File). For the data in Fig 2, ^{13}C polarization was prepared by DQ-CP transfer with a constant ^{13}C RF field strength of ~$2\nu_R/5$ and a downward-ramped ^1H RF field with an average strength of ~$3\nu_R/5$, using a contact time of 1.5 ms. Similar conditions, but with an upward ^1H ramp, were used to transfer ^{13}C polarization back to ^1H for the ^1H detection experiments in Fig 2a. The maximum t_1 and t_2 periods for Fig 2(a) and 2(b) were 5 ms and 10 ms, respectively. The recycle delay was set to 0.54 s for SAIL-Ubq, which had relatively short ^1H T_1 values (~0.25 s). For data processing, the indirect time-domain data along the t_1 period were extended to 10 ms by linear prediction.

The 3D data in Fig 3 were obtained with a recycle delay of 0.52 s using the DQ—CP scheme (Fig C in S1 File) used for Fig 2a. After the t_1 period for ^{13}C evolution, the fpRFDR sequence[40] was employed for ^{13}C–^{13}C mixing. Subsequently, the ^{13}C signal was recorded in the t_2 period. Then, the ^1H signal was acquired after DQ—CP transfer of the ^{13}C polarization to ^1H spins with a contact time of 0.5 ms. The signals were collected with maximum t_1 and t_2 periods of 2.4 ms and an acquisition period (t_3) of 10.2 ms. The relatively short t_1 and t_2 periods were employed to optimize the sensitivity for the detection of weak deuterated $^{13}C_\alpha$ signals. The t_1 and t_2 data were extended to 3.6 ms by linear prediction and was processed as discussed above for Fig 2.

Supporting Information

S1 File. Fig. A, Spinning speed dependence of ^1H MAS SSNMR of SAIL-threonine (SAIL-Thr) with its chemical structure and labeling scheme. The ^1H NMR spectra were obtained using WALTZ-16 ^{13}C decoupling with an RF field strength of 10 kHz. All the spectra were obtained with 2 scans with a pulse delay of 15 s, and the data were processed without any window function. The ^1H line widths for H_α, H_β, H_γ OH/NH are 0.22 ppm, 0.22 ppm, 0.24 ppm, 0.20 ppm, respectively. **Fig. B, A pulse sequence for ^1H-detected 2D $^1H/^{13}C$ chemical-shift correlation spectroscopy used for Fig 2a.** In this sequence, ^{13}C spin polarization was

prepared with adiabatic double-quantum cross polarization (DQ-CP) using an amplitude-modulated shaped pulse with a downward tangential ramp for the ^{1}H channel and a rectangular pulse for the ^{13}C channel. The ^{1}H RF field strength was swept from 66.0 kHz to 26.4 kHz with the average rf field set at 46.2 kHz ($\sim$3ν_R/5) while the ^{13}C RF field amplitude was kept constant at 32.0 kHz ($\sim$2ν_R/5). The contact time of the first CP was 1.5ms. During the t_1 period, SPINAL-64 ^{1}H decoupling[38] and WALTZ-16 ^{2}H decoupling were applied with RF field strengths of 10 kHz and 5 kHz, respectively. The t_1 period was incremented up to 5.1 ms with an increment of 37 µs. After the t_1 period, a pair of π/2-pulses were applied as a Z-filter in order to select the real or imaginary component of the ^{13}C polarization, which was transferred back to ^{1}H spins with the second adiabatic CP using a reversed upward tangential ramp for the ^{1}H channel and the same rectangular pulse for the ^{13}C channel. The contact time of the second CP was 1.5 ms. During the acquisition (t_2) period of 10.2 ms, ^{1}H signals were acquired with dwell times of 5 µs under ^{13}C decoupling using WALTZ-16 sequence[41] with an RF field strength of 10 kHz. The phase cycles for the pulse sequence were as follows: ϕ_1 = y; ϕ_2 = x; ϕ_3 = x, x, -x, -x; ϕ_4 = y, y, y, y, -y, -y, -y, -y; ϕ_5 = x; ϕ_6 = y, -y; ϕ_7 = y; ϕ_8 = x, -x, -x, x, -x, x, x, -x. The phase ϕ_3 and the receiver phase were incremented along the t_1 points using the States-TPPI data collection mode. **Fig. C, A pulse sequence used for ^{13}C-detected 2D ^{1}H/^{13}C chemical-shift correlation spectroscopy in [Fig 2b](#)**. A pulse sequence used for ^{13}C-detected 2D ^{1}H/^{13}C chemical-shift correlation spectroscopy in [Fig 2b](#). After excitation by a π/2-pulse, ^{1}H spin polarization evolved under ^{1}H chemical-shift interactions during the t_1 period under WALTZ-16 ^{13}C decoupling with an RF field strength of 10 kHz. The t_1 period was incremented up to 5.1 ms with a t_1 increment of 0.15 ms. The ^{1}H polarization was transferred to the ^{13}C spins by adiabatic tangential double-quantum cross polarization (DQ-CP), which was identical to the first CP scheme in Fig B in S1 File. The contact time for CP was 1.5ms. During the acquisition (t_2) period of 10.2 ms, SPINAL-64 ^{1}H decoupling and WALTZ-16 ^{2}H decoupling were applied with RF strengths of 10 kHz and 5 kHz, respectively. The t_2 dwell time was 5 µs. The phase cycles for the pulse sequence were as follows: ϕ_1 = y, -y; ϕ_2 = x, x, -x, -x; ϕ_3 = y; ϕ_4 = x, -x, -x, x. The phase ϕ_1 and the receiver phase were incremented along the t_1 points using the States-TPPI data collection mode. **Fig. D, A pulse sequence used for ^{1}H-detected 3D ^{13}C/^{13}C/^{1}H correlation spectroscopy in [Fig 3](#)**. ^{13}C spin polarization was prepared by adiabatic double-quantum cross polarization (DQ-CP) using the same parameters as discussed in Fig B in S1 File. During the t_1 period, SPINAL-64 ^{1}H decoupling and WALTZ-16 ^{2}H decoupling were applied with RF field strengths of 10 kHz and 5 kHz, respectively. After the t_1 period, a transverse component of the ^{13}C polarization was stored along the z-axis and the unnecessary component in the transverse plane is dephased during a z-filter period τ of 2 ms. Then, ^{13}C polarization transfer was achieved by ^{13}C-^{13}C dipolar couplings using the fpRFDR sequence without ^{1}H rf irradiation. A π-pulse train with the XY-16 phase cycle was rotor-synchronously applied to the ^{13}C channel so that a π-pulse was applied at the center of every rotor cycle. The π-pulse width in the fpRFDR mixing was 6.6 µs, and n = 96. After a z-filter and excitation by a π/2-pulse, ^{13}C signals were recorded during the t_2 period under SPINAL-64 ^{1}H decoupling and WALTZ-16 ^{2}H decoupling, as mentioned above for the t_1 period. Then, a transverse component of the ^{13}C polarization was transferred back to ^{1}H spins by an adiabatic DQ-CP scheme before the acquisition of ^{1}H signals in the t_3 period. The ^{1}H RF field strength was swept from 26.4 kHz to 66.0 kHz with the average rf field at 46.2 kHz ($\sim$3ν_R/5) while the ^{13}C RF field amplitude was set kept constant at 32.0 kHz ($\sim$2ν_R/5). The contact time of the second CP period was 0.5 ms. The t_1 and t_2 periods were both incremented up to 2.4 ms with an increment of 75 µs. The t_3 acquisition time was 10.2 ms with 5 µs dwell time. The phase cycles for the pulse sequence were as follows: ϕ_1 = y; ϕ_2 = x; ϕ_3 = x, x, -x, -x; ϕ_4 = y, y, y, y, -y, -y, -y, -y; ϕ_5 = y; ϕ_6 = x, -x; ϕ_7 = x; ϕ_8 = x, -x, -x, x, -x, x, x, -x. The phases ϕ_3 and ϕ_5 and the receiver phase were

incremented along the t_1 and t_2 points using the States-TPPI data collection mode. **Fig. E, a) ^{1}H-detected ^{13}C/^{1}H 2D correlation and b) ^{13}C-detected ^{13}C/^{1}H 2D correlation, and c) 1D ^{13}C CP-MAS spectra of SAIL-Ile respectively**. 1D slices at various ^{1}H chemical shifts (indicated in the fig.) from the ^{1}H and ^{13}C detected 2D ^{13}C/^{1}H correlation spectra are compared. The 1D slices and 1D spectrum in (c) are scaled so that all the 1D spectra show a common noise level for sensitivity comparisons. The experimental time was 5 min each. The pulse sequences used for (a) ^{13}C-detected and (b) ^{1}H-detected 2D ^{1}H/^{13}C chemical-shift correlation experiments are shown in Fig C and Fig B in S1 File, respectively. The CP and decoupling conditions for these experiments were similar to those for the data for the SAIL Ile labeled ubiquitin sample in [Fig 2](). The ^{13}C detection/evolution periods was 10 ms, while ^{1}H detection/evolution periods was 6.5 ms for a) and b). These periods were matched to the inverse of the average line widths of ^{13}C and ^{1}H. Although ^{1}H T_1 value for this sample was ~3 s, the recycle delay was set to 0.3 s as sufficient signal-to-noise ratios can be obtained for all of (a-c). All the spectra in Fig. E were processed with 45°- and 60°-shifted sinebell functions on the ^{1}H and ^{13}C dimensions respectively without linear prediction. **Fig. F, A comparison of 1D ^{13}C MAS spectra of SAIL-Ile by a) π/2-pulse direct excitation and b) cross-polarization (CP) from ^{1}H spins**. The pulse sequence for cross polarization experiments used in (b) was the same as showed in Fig C in S1 File except that the t_1 value was set to 0.1 μs and t_2 was used as an acquisition period. The cross polarization transfer was optimized for protonated carbons for ^{1}H-detected experiments. The ^{1}H RF field strength was swept from 70.0 kHz to 28.0 kHz with the average rf field set at 49.0 kHz (~$5\nu_R$/8) while the ^{13}C RF field strength was kept constant at 30.0 kHz (~$3\nu_R$/8). The contact time of CP was 1.5 ms. The ^{13}C detection periods was 3.1 ms for both (a) and (b). Recycle delays were set to 6000 s and 20 s for (a) and (b), respectively. The long delays were employed to ensure that the signals were fully recovered. No window functions were applied to the spectra. The CP-transfer efficiency for C_α, C_β, $C_{\gamma1}$, $C_{\gamma2}$ and C_δ were 55%, 60%, 68%, 45% and 40%, respectively. The values were obtained by dividing the ratio of the integral peak intensity in (b) to that of the corresponding peak in (a) by γ_H/γ_C, where γ_H and γ_C are the gyromagnetic ratios of ^{1}H and ^{13}C, respectively. **Table A, The comparison of S/N for ^{1}H-detected 2D ^{13}C/^{1}H correlation, ^{13}C-detected ^{13}C/^{1}H correlation, and ^{13}C 1D CPMAS experiments of the SAIL-Ile labeled ubiquitin sample. Table B, The comparison of signal-to-noise ratios (S/N) for ^{1}H-detected 2D ^{13}C/^{1}H correlation, ^{13}C-detected ^{13}C/^{1}H correlation, and ^{13}C 1D CPMAS experiments of SAIL Ile sample. Table C, Preliminary ^{1}H and ^{13}C signal assignments of SAIL-Ile labeled ubiquitin**.
(PDF)

Author Contributions

Conceived and designed the experiments: SW SP MK YI. Performed the experiments: SW SP YN YE TN KY MT YI. Analyzed the data: SW SP YI. Contributed reagents/materials/analysis tools: SW SP YN YE TN KY TA MT TT MK YI. Wrote the paper: SW SP YN YE TN KY TA MT TT MK YI.

References

1. Ishii Y, Tycko R. Sensitivity enhancement in solid state N-15 NMR by indirect detection with high-speed magic angle spinning. J. Magn. Reson. 2000; 142(1):199–204. PMID: [10617453]()

2. Ishii Y, Yesinowski JP, Tycko R. Sensitivity enhancement in solid-state C-13 NMR of synthetic polymers and biopolymers by H-1 NMR detection with high-speed magic angle spinning. J. Am. Chem. Soc. 2001; 123(12):2921–2922. PMID: [11456995]()

3.   Paulson EK, Morcombe CR, Gaponenko V, Dancheck B, Byrd RA, Zilm KW. Sensitive high resolution inverse detection NMR spectroscopy of proteins in the solid state. J. Am. Chem. Soc. 2003; 125(51):15831–15836. PMID: 14677974

4.   Schnell I, Saalwachter K. N-15-H-1 bond length determination in natural abundance by inverse detection in fast-MAS solid-state NMR spectroscopy. J. Am. Chem. Soc. 2002; 124(37):10938–10939. PMID: 12224915

5.   Chevelkov V, Rehbein K, Diehl A, Reif B. Ultrahigh resolution in proton solid-state NMR spectroscopy at high levels of deuteration. Angew. Chem. Int. Edit. 2006; 45(23):3878–3881. PMID: 16646097

6.   Reif B. Ultra-high resolution in MAS solid-state NMR of perdeuterated proteins: Implications for structure and dynamics. J. Magn. Reson. 2012; 216:1–12. doi: 10.1016/j.jmr.2011.12.017 PMID: 22280934

7.   Zhou DH, Shah G, Cormos M, Mullen C, Sandoz D, Rienstra CM. Proton-detected solid-state NMR spectroscopy of fully protonated proteins at 40 kHz magic angle spinning. J. Am. Chem. Soc. 2007; 129:11791–11801. PMID: 17725352

8.   Knight MJ, Webber AL, Pell AJ, Guerry P, Barbet-Massin E, Bertini I, et al. Fast Resonance Assignment and Fold Determination of Human Superoxide Dismutase by High-Resolution Proton-Detected Solid-State MAS NMR Spectroscopy. Angew. Chem.-Int Edit. 2011; 50(49):11697–11701. doi: 10.1002/anie. 201106340 PMID: 21998020

9.   Barbet-Massin E, Pell AJ, Retel JS, Andreas LB, Jaudzems K, Franks WT, et al. Rapid Proton-Detected NMR Assignment for Proteins with Fast Magic Angle Spinning. J. Am. Chem. Soc. 2014; 136:12489–12497. doi: 10.1021/ja507382j PMID: 25102442

10. Marchetti A, Jehle S, Felletti M, Knight MJ, Wang Y, Xu Z-Q, et al. Backbone Assignment of Fully Protonated Solid Proteins by 1H Detection and Ultrafast Magic-Angle-Spinning NMR Spectroscopy. Angew. Chem. Int. Edit. 2012; 51(43):10756–10759. doi: 10.1002/anie.201203124 PMID: 23023570

11. Ishii Y, Yesinowski JP, Tycko R. Sensitivity enhancement in solid-state C-13 NMR of synthetic polymers and biopolymers by H-1 NMR detection with high-speed magic angle spinning. J. Am. Chem. Soc. 2001; 123(12):2921–2922. PMID: 11456995

12. Guo C, Hou G, Lu X, O'Hare B, Struppe J, Polenova T. Fast magic angle spinning NMR with heteronucleus detection for resonance assignments and structural characterization of fully protonated proteins. J. Biomol. NMR. 2014; 60(4):219–229. doi: 10.1007/s10858-014-9870-y PMID: 25381566

13. Kainosho M, Torizawa T, Iwashita Y, Terauchi T, Ono AM, Guntert P. Optimal isotope labelling for NMR protein structure determinations. Nature. 2006; 440(7080):52–57. PMID: 16511487

14. Takahashi H, Kainosho M, Akutsu H, Fujiwara T. H-1-detected H-1-H-1 correlation spectroscopy of a stereo-array isotope labeled amino acid under fast magic-angle spinning. J. Magn. Reson. 2010; 203(2):253–256. doi: 10.1016/j.jmr.2010.01.005 PMID: 20129804

15. Parathasarathy S, Nishiyama Y, Ishii Y. Sensitivity and resolution enhanced solid-state NMR for paramagnetic systems and biomoleculesunder very fast magic agle spinning. Acc. Chem. Res. 2013; 46:2127–2135. doi: 10.1021/ar4000482 PMID: 23889329

16. Kainosho M, Guentert P. SAIL—stereo-array isotope labeling. Q. Rev. Biophys. 2009; 42(4):247–300. doi: 10.1017/S0033583510000016 PMID: 20370954

17. Torii K, Iitaka Y. Crystal structure of L-isoleucine. Acta Crystallographica Section B-Structural Crystallography and Crystal Chemistry. 1971; B 27(NOV15):2237-&.

18. Varughese KI, Srinivasan R. Studies in molecular-structure, symmetry and conformation. 14. Crystal and molecular-structure of L-isoleucine hydrochloride monohydrate form-2. Pramana. 1976; 6(4):189–195.

19. Wickramasinghe NP, Parthasarathy S, Jones CR, Bhardwaj C, Long F, Kotecha M, et al. Nanomole-scale protein solid-state NMR by breaking intrinsic H-1 T-1 boundaries. Nature Methods. 2009; 6(3):215–218. doi: 10.1038/nmeth.1300 PMID: 19198596

20. Igumenova TI, McDermott AE, Zilm KW, Martin RW, Paulson EK, Wand AJ. Assignments of carbon NMR resonances for microcrystalline ubiquitin. J. Am. Chem. Soc. 2004; 126(21):6720–6727. PMID: 15161300

21. Huber M, Boeckmann A, Hiller S, Meier BH. 4D solid-state NMR for protein structure determination. Physical Chemistry Chemical Physics. 2012; 14(15):5239–5246. doi: 10.1039/c2cp23872a PMID: 22402636

22. Nadaud PS, Helmus JJ, Sengupta I, Jaroniec CP. Rapid Acquisition of Multidimensional Solid-State NMR Spectra of Proteins Facilitated by Covalently Bound Paramagnetic Tags. J. Am. Chem. Soc. 2010; 132(28):9561–9563. doi: 10.1021/ja103545e PMID: 20583834

23. Althaus SM, Mao K, Stringer JA, Kobayashi T, Pruski M. Indirectly detected heteronuclear correlation solid-state NMR spectroscopy of naturally abundant N-15 nuclei. Solid State Nucl. Magn. Reson. 2014; 57–58:17–21. doi: 10.1016/j.ssnmr.2014.10.003 PMID: 25466354

24. Suiter CL, Paramasivam S, Hou G, Sun S, Rice D, Hoch JC, et al. Sensitivity gains, linearity, and spectral reproducibility in nonuniformly sampled multidimensional MAS NMR spectra of high dynamic range. J. Biomol. NMR. 2014; 59(2):57–73. doi: 10.1007/s10858-014-9824-4 PMID: 24752819

25. Kobayashi T, Mao K, Paluch P, Nowak-Krol A, Sniechowska J, Nishiyama Y, et al. Study of Intermolecular Interactions in the Corrole Matrix by Solid-State NMR under 100 kHz MAS and Theoretical Calculations. Angew. Chem. Int. Edit. 2013; 52(52):14108–14111. doi: 10.1002/anie.201305475 PMID: 24227750

26. Nishiyama Y, Malon M, Ishii Y, Ramamoorthy A. 3D N-15/N-15/H-1 chemical shift correlation experiment utilizing an RFDR-based H-1/H-1 mixing period at 100 kHz MAS. J. Magn. Reson. 2014; 244:1–5. doi: 10.1016/j.jmr.2014.04.008 PMID: 24801998

27. Rienstra CM, Tucker-Kellogg L, Jaroniec CP, Hohwy M, Reif B, McMahon MT, et al. De novo determination of peptide structure with solid-state magic-angle spinning NMR spectroscopy. Proc. Natl. Acad. Sci. U. S. A. 2002; 99(16):10260–10265. PMID: 12149447

28. Heise H, Hoyer W, Becker S, Andronesi OC, Riedel D, Baldus M. Molecular-level secondary structure, polymorphism, and dynamics of full-length alpha-synuclein fibrils studied by solid-state NMR. Proc. Natl. Acad. Sci. U. S. A. 2005; 102(44):15871–15876. PMID: 16247008

29. Wasmer C, Lange A, Van Melckebeke H, Siemer AB, Riek R, Meier BH. Amyloid fibrils of the HET-s(218–289) prion form a beta solenoid with a triangular hydrophobic core. Science. 2008; 319(5869):1523–1526. doi: 10.1126/science.1151839 PMID: 18339938

30. Helmus JJ, Surewicz K, Nadaud PS, Surewicz WK, Jaroniec CP. Molecular conformation and dynamics of the Y145Stop variant of human prion protein. Proc. Natl. Acad. Sci. U. S. A. 2008; 105(17):6284–6289. doi: 10.1073/pnas.0711716105 PMID: 18436646

31. Schneider R, Schumacher MC, Mueller H, Nand D, Klaukien V, Heise H, et al. Structural Characterization of Polyglutamine Fibrils by Solid-State NMR Spectroscopy. J. Mol. Biol. 2011; 412(1):121–136. doi: 10.1016/j.jmb.2011.06.045 PMID: 21763317

32. Lu J-X, Qiang W, Yau W-M, Schwieters CD, Meredith SC, Tycko R. Molecular Structure of beta-Amyloid Fibrils in Alzheimer's Disease Brain Tissue. Cell. 2013; 154(6):1257–1268. doi: 10.1016/j.cell.2013.08.035 PMID: 24034249

33. Hoop CL, Lin H-K, Kar K, Hou Z, Poirier MA, Wetzel R, et al. Polyglutamine amyloid core boundaries and flanking domain dynamics in huntingtin fragment fibrils determined by solid-state nuclear magnetic resonance. Biochemistry. 2014; 53(42):6653–6666. doi: 10.1021/bi501010q PMID: 25280367

34. Goobes G, Goobes R, Schueler-Furman O, Baker D, Stayton PS, Drobny GP. Folding of the C-terminal bacterial binding domain in statherin upon adsorption onto hydroxyapatite crystals. Proc. Natl. Acad. Sci. U. S. A. 2006; 103(44):16083–16088. PMID: 17060618

35. Vyalikh A, Simon P, Rosseeva E, Buder J, Kniep R, Scheler U. Intergrowth and Interfacial Structure of Biomimetic Fluorapatite- Gelatin Nanocomposite: A Solid-State NMR Study. J. Phys. Chem. B. 2014; 118(3):724–730. doi: 10.1021/jp410299x PMID: 24354406

36. Lange A, Scholz I, Manolikas T, Ernst M, Meier BH. Low-power cross polarization in fast magic-angle spinning NMR experiments. Chem. Phys. Lett. 2009; 468(1–3):100–105.

37. Kotecha M, Wickramasinghe NP, Ishii Y. Efficient low-power heteronuclear decoupling in 13C high-resolution solid-state NMR under fast magic angle spinning. Magn. Reson. Chem. 2007; 45:S221–230. doi: 10.1002/mrc.2151 PMID: 18157841

38. Fung BM, Khitrin AK, Ermolaev K. An improved broadband decoupling sequence for liquid crystals and solids. J. Magn. Reson. 2000; 142(1):97–101. PMID: 10617439

39. Delaglio F, Grzesiek S, Vuister GW, Zhu G, Pfeifer J, Bax A. Nmrpipe—a Multidimensional Spectral Processing System Based on Unix Pipes. J. Biomol. NMR. 1995; 6(3):277–293. PMID: 8520220

40. Ishii Y. 13C-13C dipolar recoupling under very fast magic angle spinning in solid-state NMR: Applications to distance measurements, spectral assignments, and high-throughput secondary-structure elucidation. J. Chem. Phys. 2001; 114:8473–8483.

41. Shaka AJ, Keeler J, Frenkiel T, Freeman J. An improved sequence for broadband decoupling: WALTZ-16. J. Magn. Reson. 1983; 52:335–338.